Science Advances
AAAS

Supplementary Materials for

Two cooperative binding sites sensitize PI(4,5)P_2 recognition by the tubby domain

Veronika Thallmair *et al.*

Corresponding author: Sebastian Thallmair, thallmair@fias.uni-frankfurt.de;
Dominik Oliver, oliverd@staff.uni-marburg.de

Sci. Adv. **8**, eabp9471 (2022)
DOI: 10.1126/sciadv.abp9471

This PDF file includes:

Supplementary Text

Open-beta Martini 3 models for PI(4,5)P_2 and PI(4)P

The coarse-grained (CG) models for the phosphoinositols PI(4,5)P_2 and PI(4)P were built based on the refined models for Martini 2 (ref. *27* of the main text). While the bonded terms were kept unchanged, the bead type was adapted to the open-beta version of Martini 3. Table S1 lists the old (Martini 2) and new (open-beta Martini 3) bead types. Note that the bead types of the open-beta version are not identical with the final release of Martini 3 (ref. *21, 22* of the main text). The itp files in Gromacs format are publicly available within the Zenodo dataset associated with the article (doi: 10.5281/zenodo.6587156).

Comparison of tubbyCT crystal structure with modeled structures

To generate the CG model for tubbyCT, the missing loops were modeled using the I-TASSER server (*50*). Fig. S4a depicts the crystal structure (pdb code 1I7E) together with the modeled structure from I-TASSER as well as a more recent structure obtained by AlphaFold. Both modeled structures match well with the overall protein fold of the crystal structure. The residues which were not resolved in the crystal structure show some deviations between both models. The missing loop (residues 304–309) which includes parts of the novel PI(4,5)P_2 binding site is highlighted by the orange circle (Fig. S4a).

Fig. S4b shows a more detailed view on this loop including the side chain orientations of the five consecutive positively charges residues 301-305. While the orientation of the first two residues matches well with the crystal structure for both models, the third one deviates from it for both models. The last two residues (304, 305) are not present in the crystal structure and while the orientation of K304 agrees for models, the orientation of K305 deviates from each other in both models.

RMSF comparison of membrane-bound and free tubbyCT

Fig. S5a shows the comparison of the backbone root mean square fluctuations (RMSF) of membrane-bound and free tubbyCT. While most regions of the protein do not show significant differences in RMSF, three loops between residues 300–340 show reduced flexibility upon membrane binding of $\Delta\mathrm{RMSF} \approx -0.1$ nm. The first loop contains the novel binding site and indicates that PI(4,5)P_2 binding reduces the flexibility of the loop. Fig. S5(b) shows the structure of tubbyCT colored according to the RMSF difference between membrane-bound and free tubbyCT. It can be clearly recognized that the three loops are all on the same face of the protein. It is the face which is in contact with the membrane.

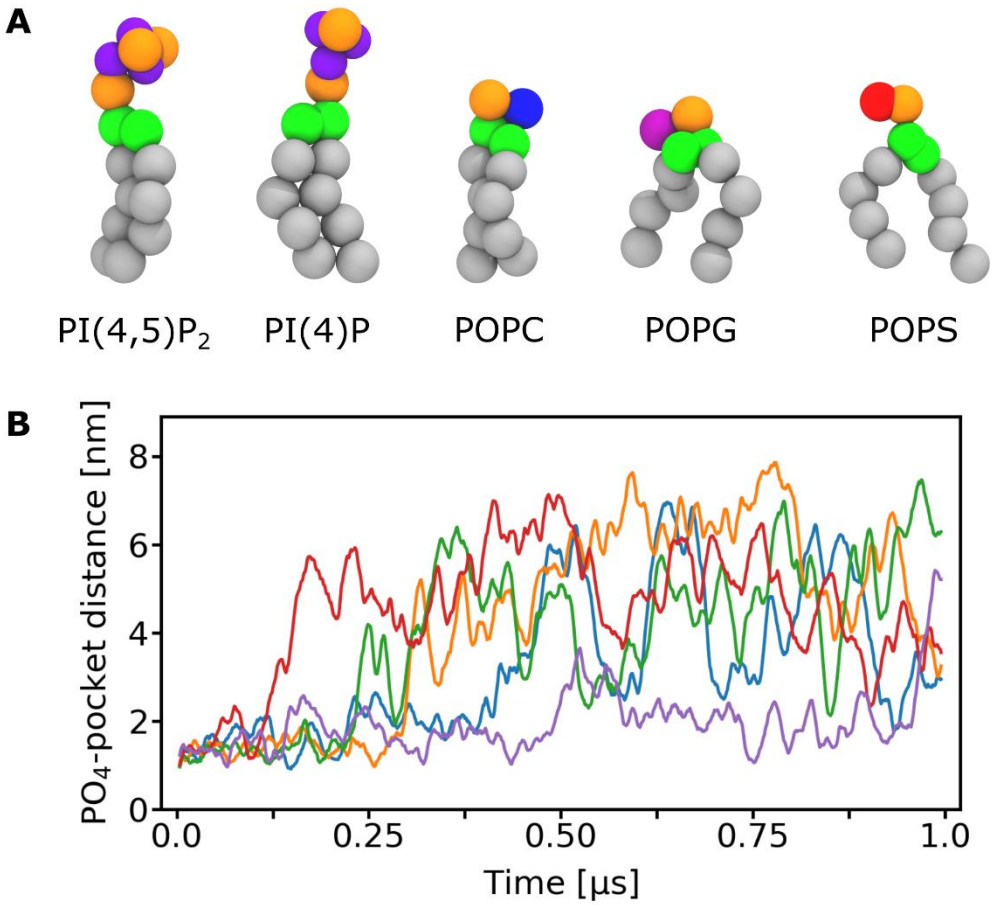

Fig. S1. Binding of a TubbyCT to a single PI(4,5)P_2 lipid embedded in a negatively charged membrane. (a) Representative snapshots of the different lipids employed in this work. The spheres depict the size of the CG beads based on their non-bonded Lennard-Jones interactions. Colors are as follows: inositol ring – purple; phosphate – orange; glycerol linker – green; aliphatic tails – grey; choline – blue; glycerol head group – magenta; serine – red. (b) Control simulations of tubbyCT bound to one PI(4,5)P_2 lipid embedded in a POPC membrane containing 5 mol% POPG (5×1 μs) with a doubly negatively charged headgroup. Therefore, the glycine moiety was considered being deprotonated and represented by a regular Qn bead with a charge of −1.

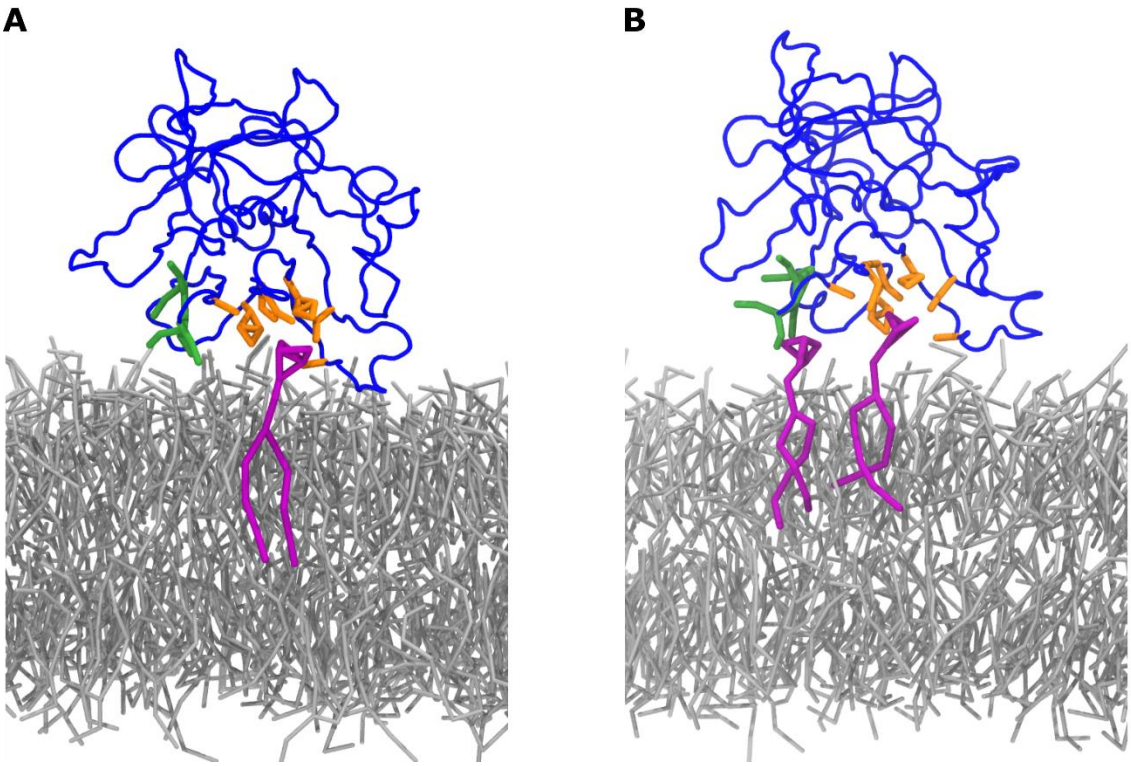

Fig. S2. Exemplary snapshots of tubbyCT binding to one and two PI(4,5)P_2 lipids, respectively. (a) TubbyCT binding to one PI(4,5)P_2. The snapshot was taken from the umbrella sampling window at the distance of the PMF minimum of 1.9 nm. The colors are: backbone of TubbyCT – blue; residues of the canonical binding site – orange; residues of the novel binding site – green; PI(4,5)P_2 – purple; POPC – grey. (b) TubbyCT binding to two PI(4,5)P_2. The snapshot was taken from the umbrella sampling window at the distance of the PMF minimum of 1.7 nm. Colors are the same as in (a).

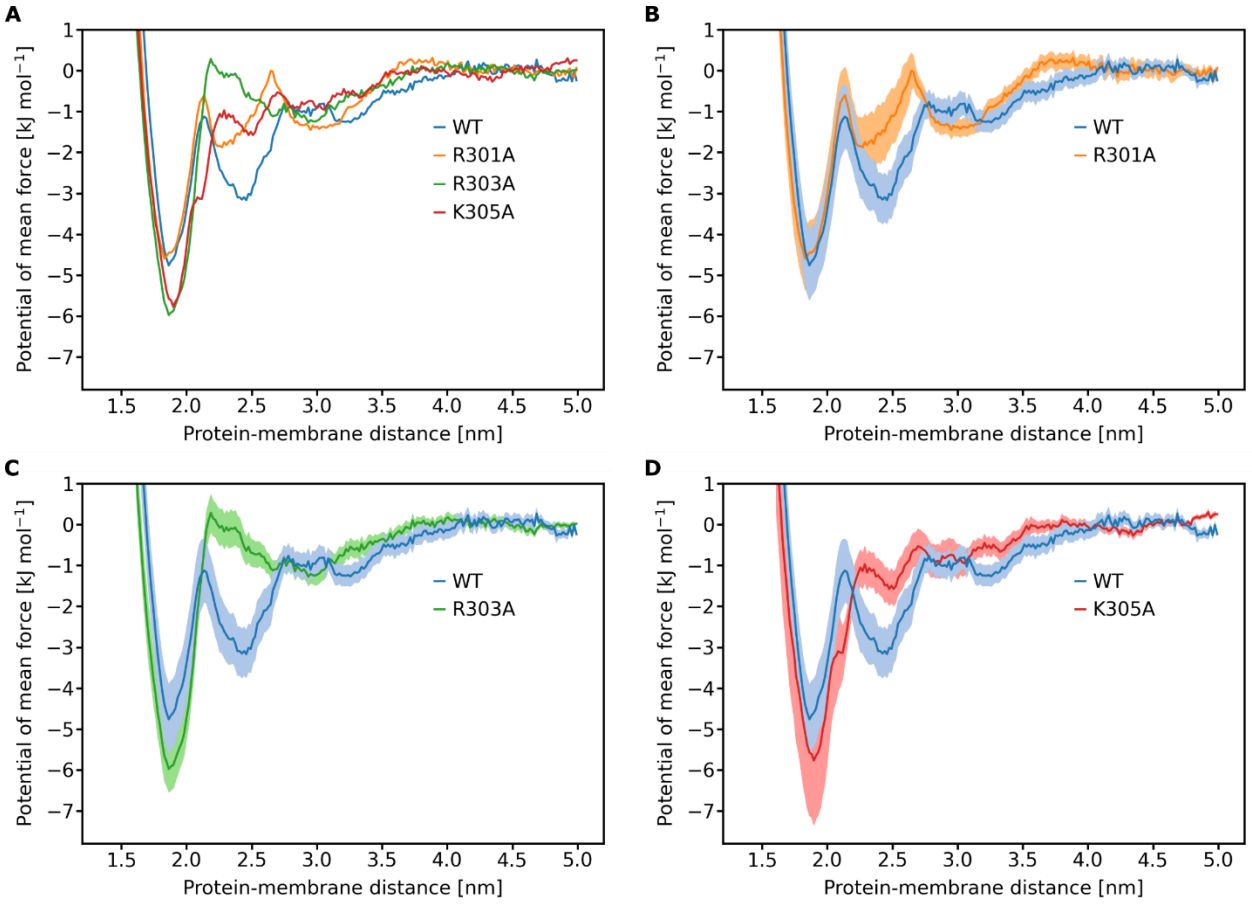

Fig. S3. PMFs for mutational analysis of the novel second binding site. (a) PMFs for the PI(4,5)P_2 binding of tubbyCT WT (blue) as well as the mutants R301A (orange), R303A (green), and K305A (red). The error bars are omitted for clarity here, but they are included in the one-to-one comparison between WT and the respective mutants (b–d). (b) PMF for the PI(4,5)P_2 binding of tubbyCT WT and R301A. For completeness, we included the R301A mutant in the comparison (see also Fig. 4d in the manuscript). (c) PMF for the PI(4,5)P_2 binding of tubbyCT WT and R303A. (d) PMF for the PI(4,5)P_2 binding of tubbyCT WT and K305A.

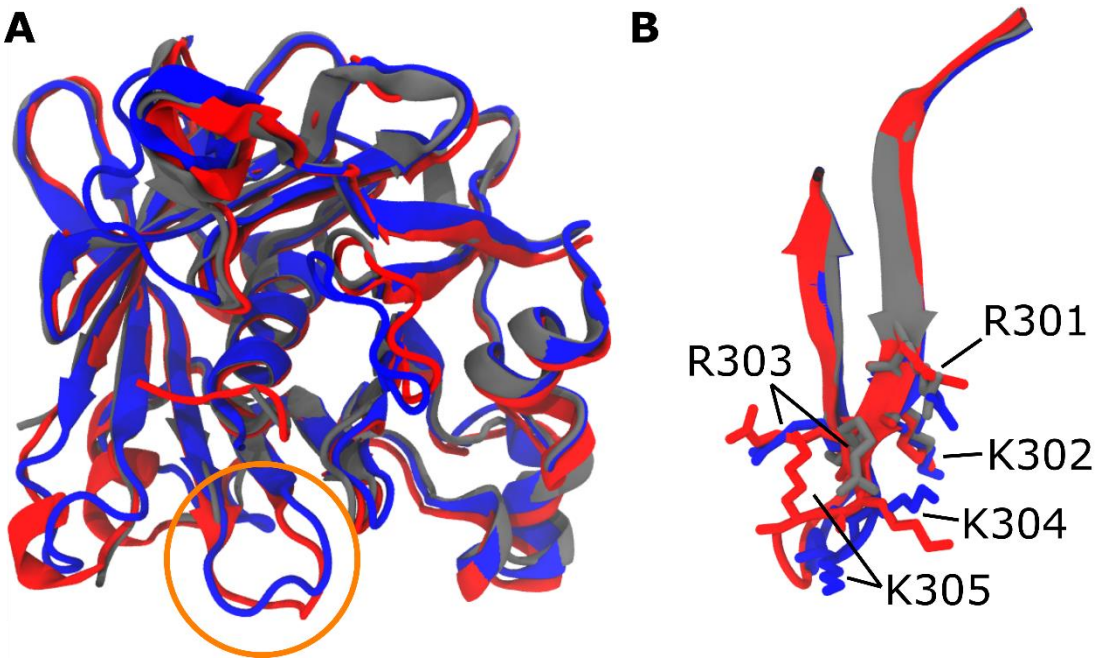

Fig. S4. Comparison of structural models for tubbyCT. (a) Overlay of the crystal structure of tubbyCT (grey, pdb code: 1I7E) with the model obtained from the I-TASSER server (blue) (ref. *50* of the main text) used as template for the missing loops here and the model obtained from AlphaFold (red) (ref. *56*, *57* of the main text). The orange circle highlights the loop with the novel second PI(4,5)P_2 binding site. The structure alignment was performed based on the Cα positions and included all residues resolved in the crystal structure. (b) Comparison of the side chain orientations of the residues 301–305 of the novel second binding site between the three structures. Note that bonds in the Gō-like model were only added between residues resolved in the crystal structure.

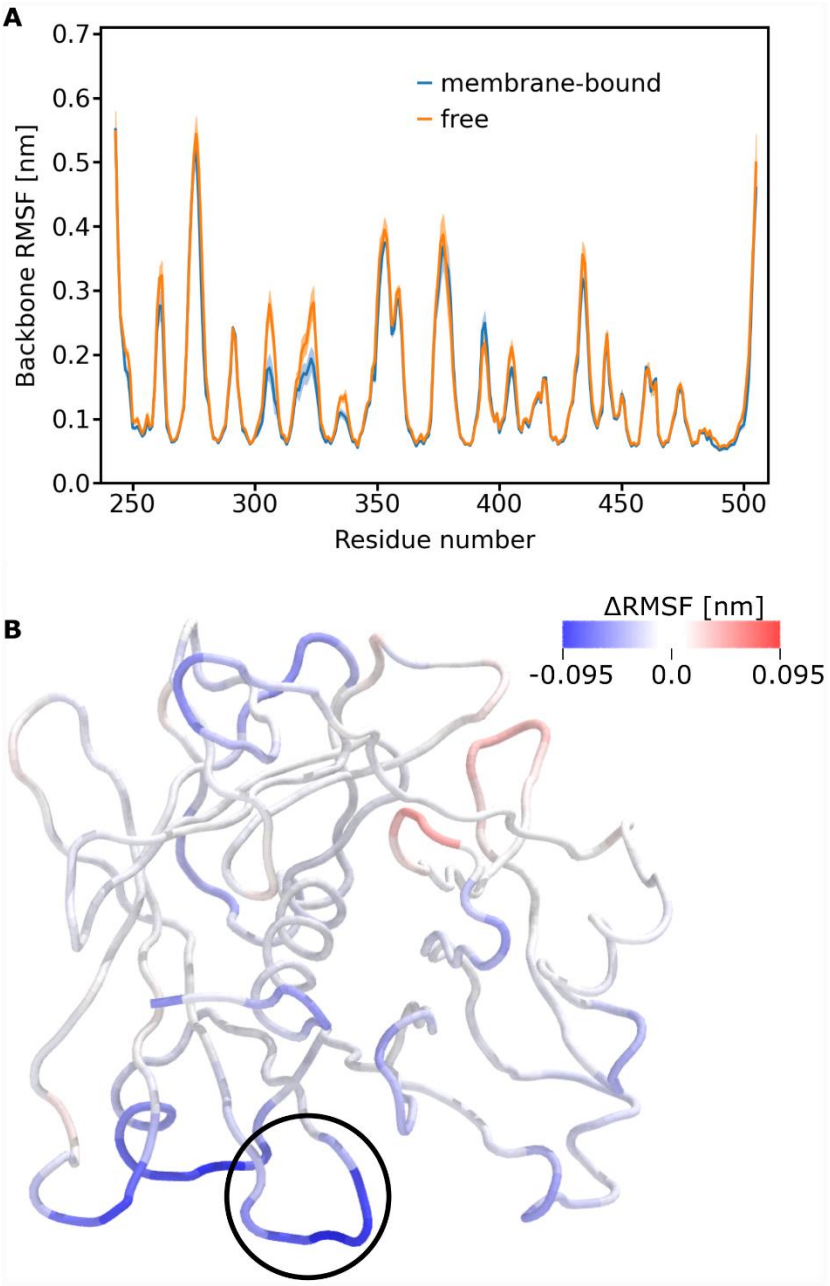

Fig. S5. Root mean square fluctuations (RMSF) of tubbyCT. (a) RMSF of the backbone beads of membrane-bound (5 mol% PI(4,5)P_2, blue) and free tubbyCT (orange). Darker lines depict the average of 10 windows of 500 ns each; shaded areas depict the standard error. (b) ΔRMSF between membrane-bound and free tubbyCT mapped on the modeled structure. Blue areas indicate reduced fluctuations upon membrane binding; red areas indicate increased fluctuations. The black circle highlights the loop with the novel second PI(4,5)P_2 binding site.

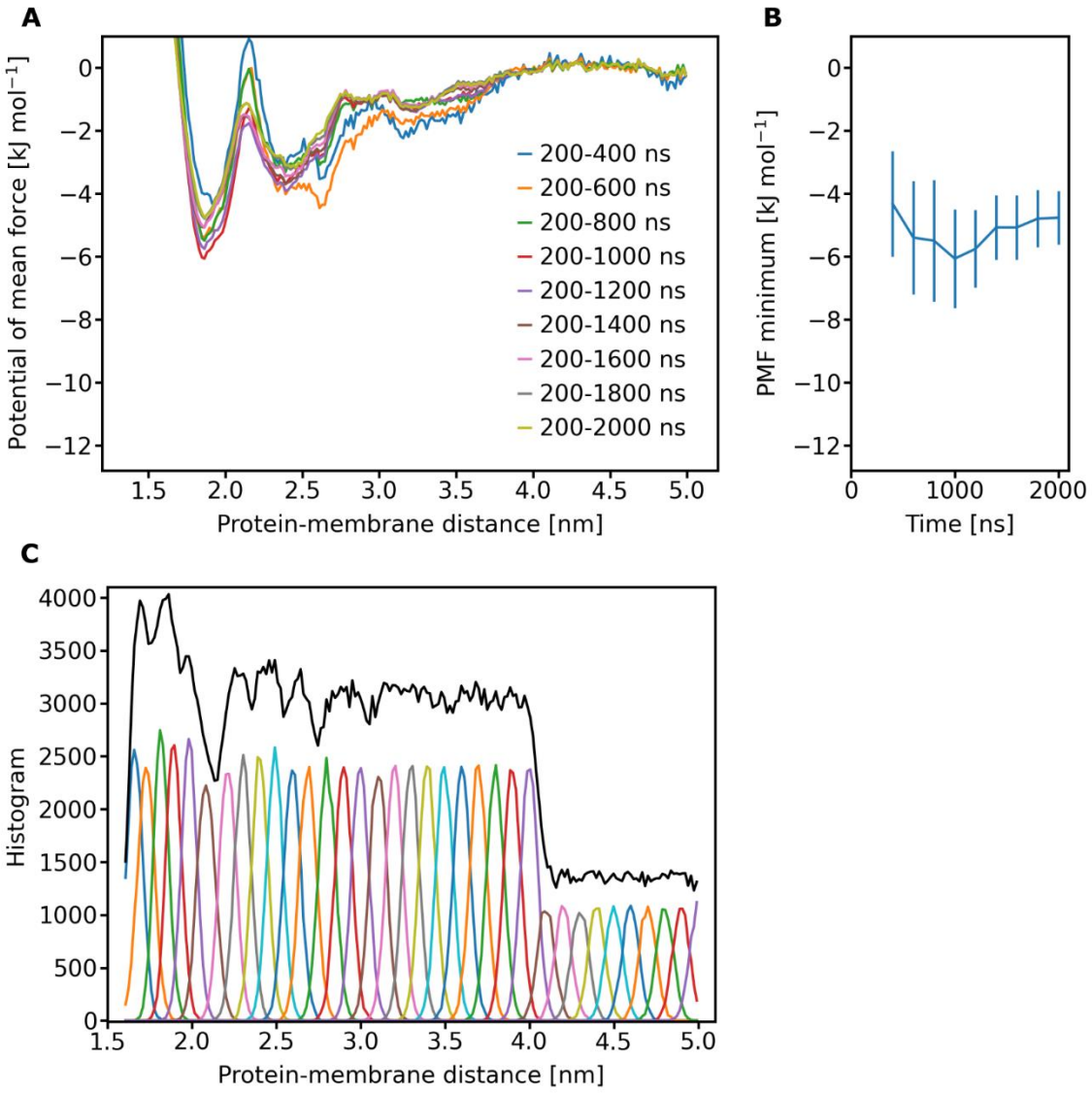

Fig. S6. Convergence analysis of the PMF calculation for tubbyCT binding to one PI(4,5)P_2 lipid. (a) PMFs calculated for different time windows from 200–400 ns to 200–2000 ns in steps of 200 ns. The initial 200 ns of each window were discarded to allow the system to equilibrate. The PMF of the final time interval of 200–2000 ns is used for further analysis. Note that for windows centered at distances ≥ 4.1 nm, the simulation time was 1 µs instead of 2 µs. (b) Energy minima from the time windows in (a) including the respective error bars. (c) Histograms of the umbrella windows (colored lines) analyzed by the *gmx wham* tool. The black line depicts the sum of the analyzed histograms.

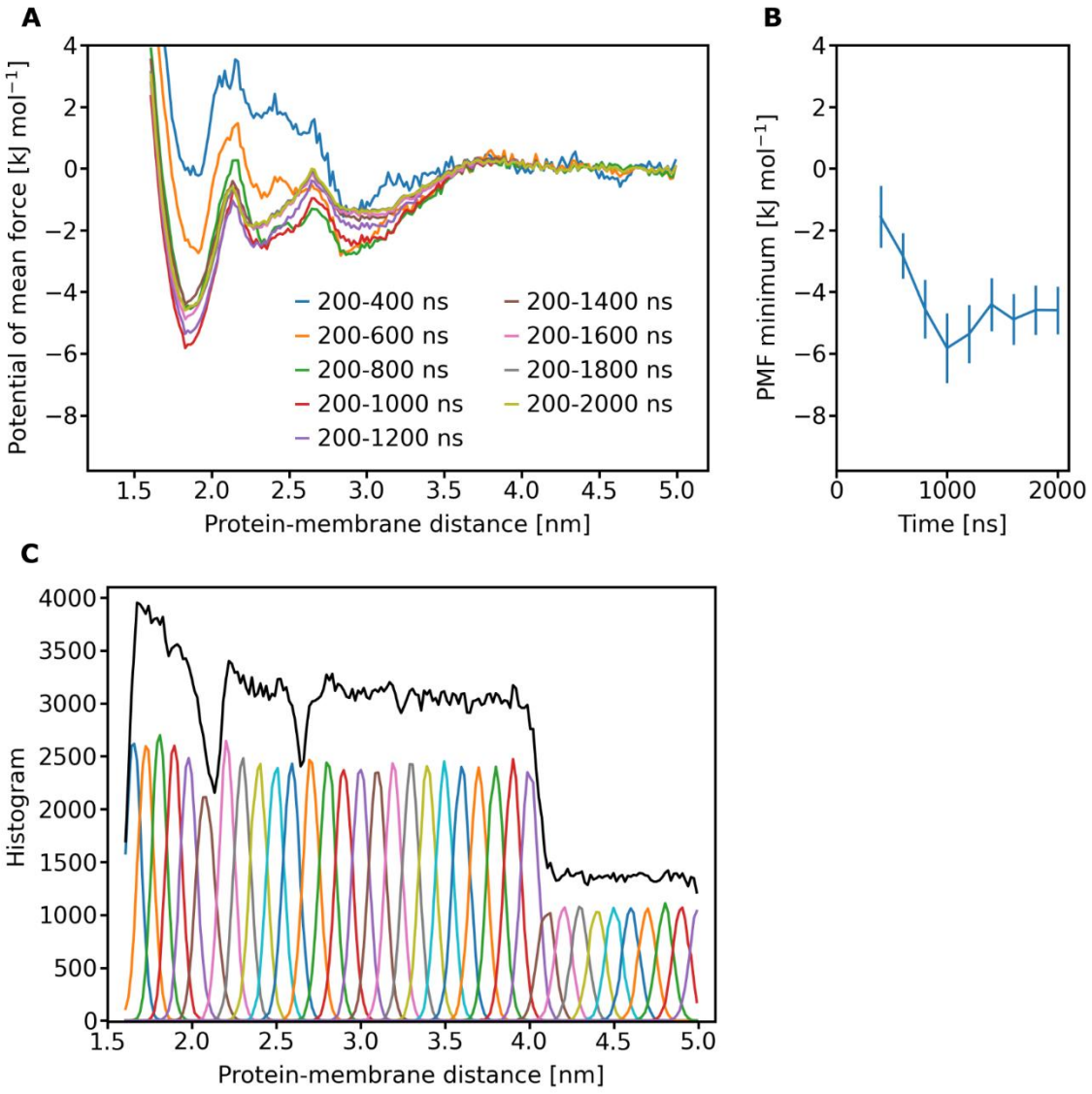

Fig. S7. Convergence analysis of the PMF calculation for R301A tubbyCT binding to one PI(4,5)P_2 lipid. (a) PMFs calculated for different time windows from 200–400 ns to 200–2000 ns in steps of 200 ns. The initial 200 ns of each window were discarded to allow the system to equilibrate. The PMF of the final time interval of 200–2000 ns is used for further analysis. Note that for windows centered at distances ≥ 4.1 nm, the simulation time was 1 µs instead of 2 µs. (b) Energy minima from the time windows in (a) including the respective error bars. (c) Histograms of the umbrella windows (colored lines) analyzed by the *gmx wham* tool. The black line depicts the sum of the analyzed histograms.

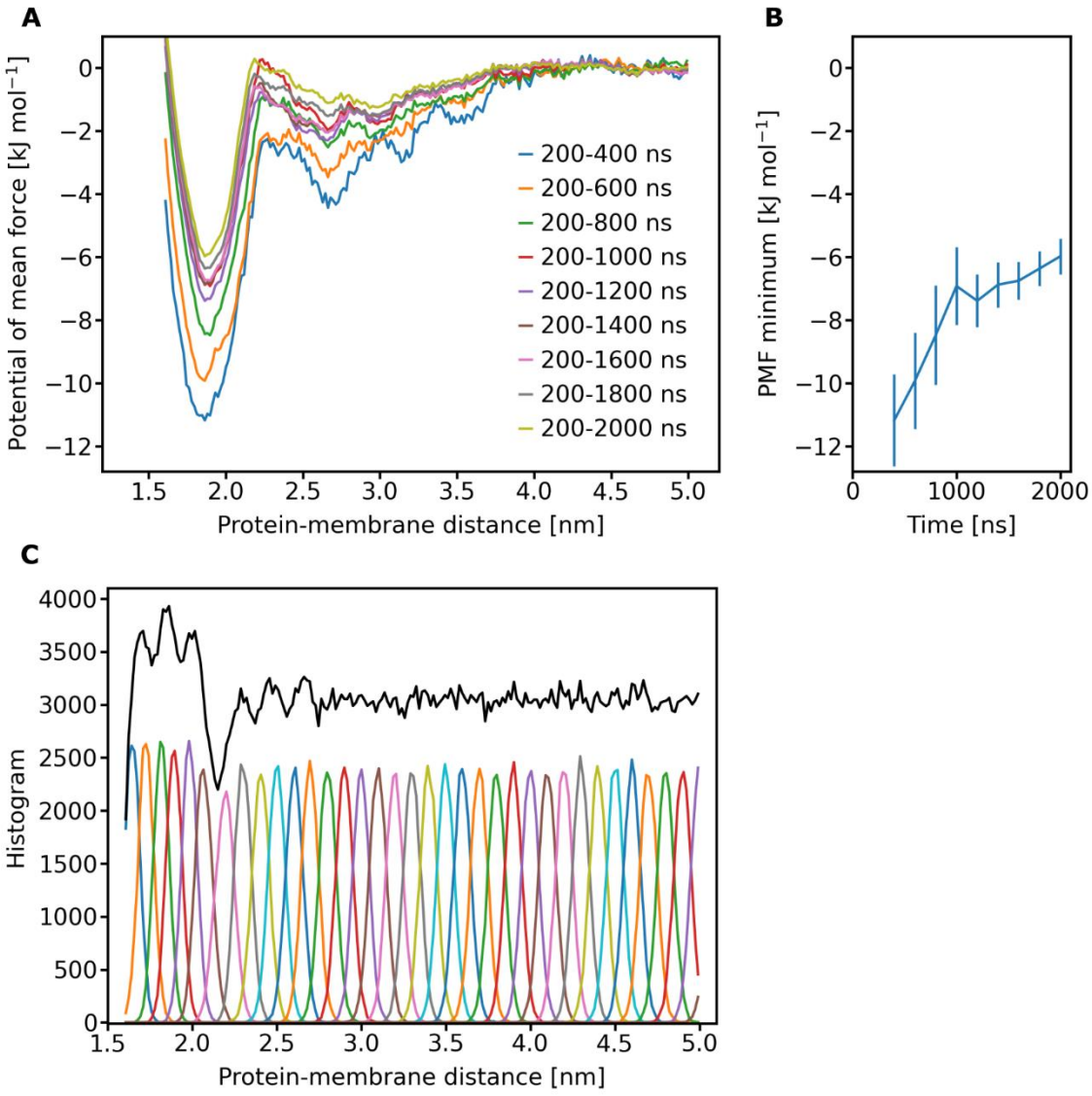

Fig. S8. Convergence analysis of the PMF calculation for R303A tubbyCT binding to one PI(4,5)P_2 lipid. (a) PMFs calculated for different time windows from 200–400 ns to 200–2000 ns in steps of 200 ns. The initial 200 ns of each window were discarded to allow the system to equilibrate. The PMF of the final time interval of 200–2000 ns is used for further analysis. (b) Energy minima from the time windows in (a) including the respective error bars. (c) Histograms of the umbrella windows (colored lines) analyzed by the *gmx wham* tool. The black line depicts the sum of the analyzed histograms.

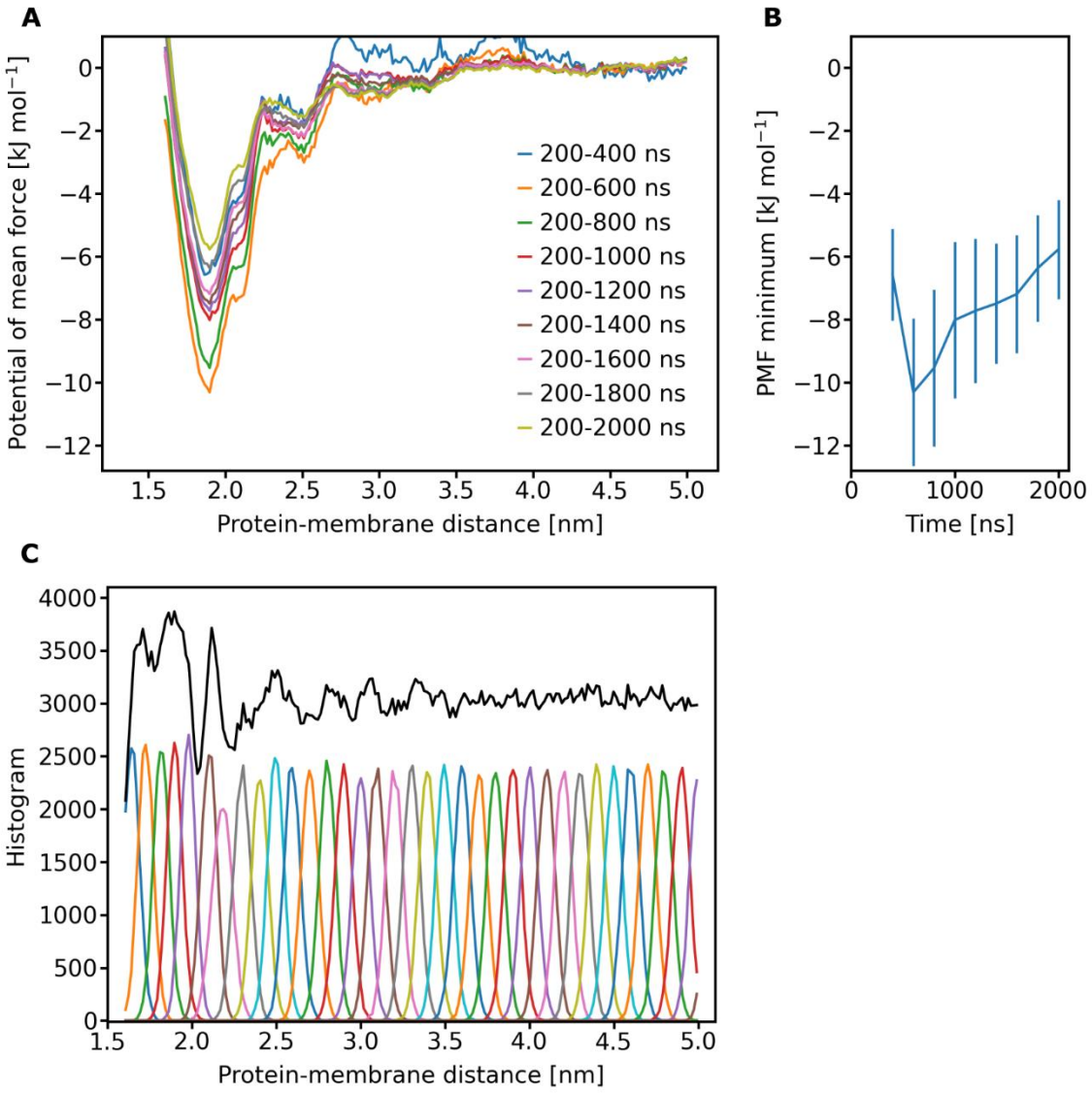

Fig. S9. Convergence analysis of the PMF calculation for K305A tubbyCT binding to one PI(4,5)P_2 lipid. (a) PMFs calculated for different time windows from 200–400 ns to 200–2000 ns in steps of 200 ns. The initial 200 ns of each window were discarded to allow the system to equilibrate. The PMF of the final time interval of 200–2000 ns is used for further analysis. (b) Energy minima from the time windows in (a) including the respective error bars. (c) Histograms of the umbrella windows (colored lines) analyzed by the *gmx wham* tool. The black line depicts the sum of the analyzed histograms.

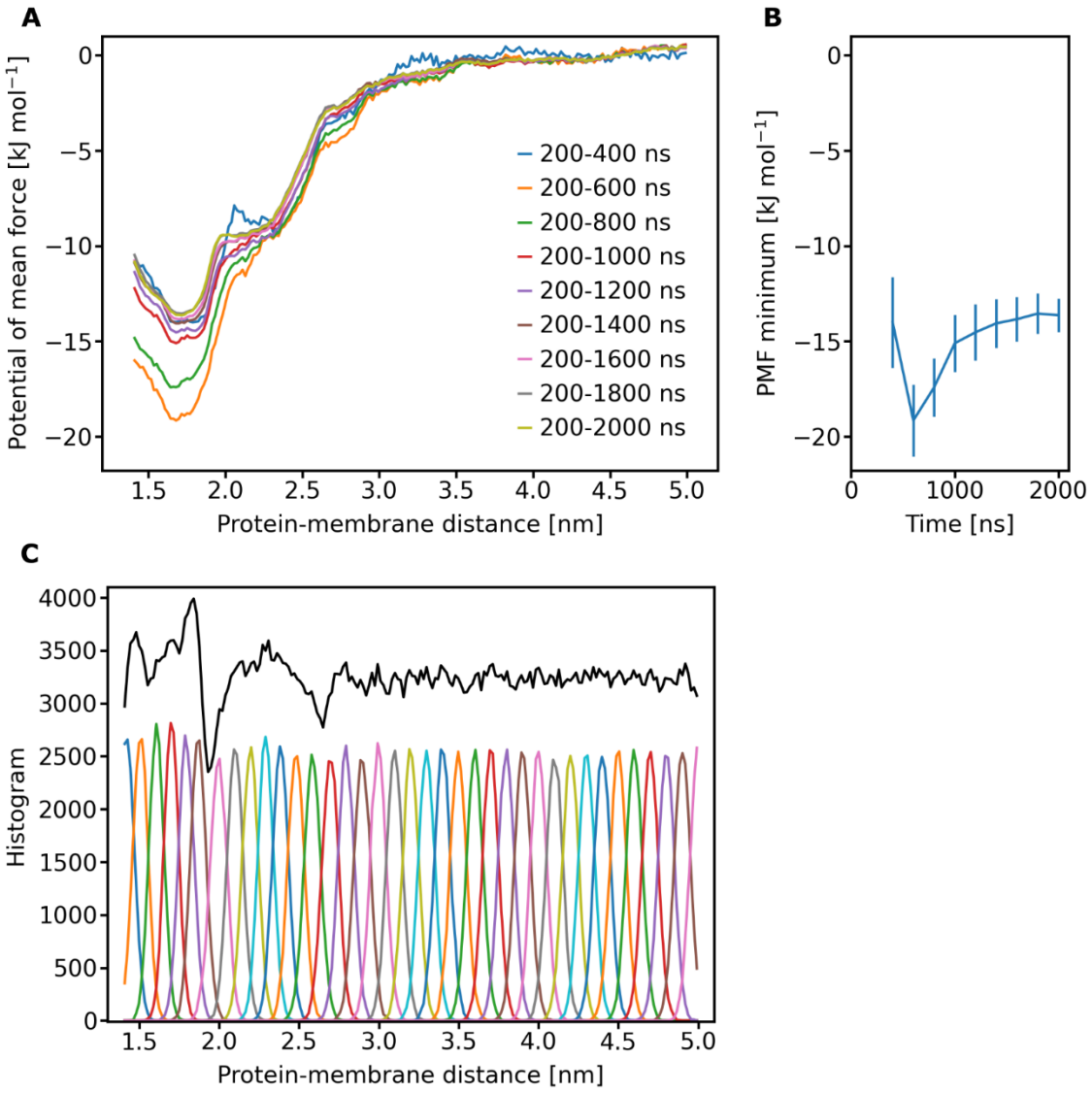

Fig. S10. Convergence analysis of the PMF calculation for tubbyCT binding to two PI(4,5)P_2 lipids. (a) PMFs calculated for different time windows from 200–400 ns to 200–2000 ns in steps of 200 ns. The initial 200 ns of each window were discarded to allow the system to equilibrate. The PMF of the final time interval of 200–2000 ns is used for further analysis. (b) Energy minima from the time windows in (a) including the respective error bars. (c) Histograms of the umbrella windows (colored lines) analyzed by the *gmx wham* tool. The black line depicts the sum of the analyzed histograms.

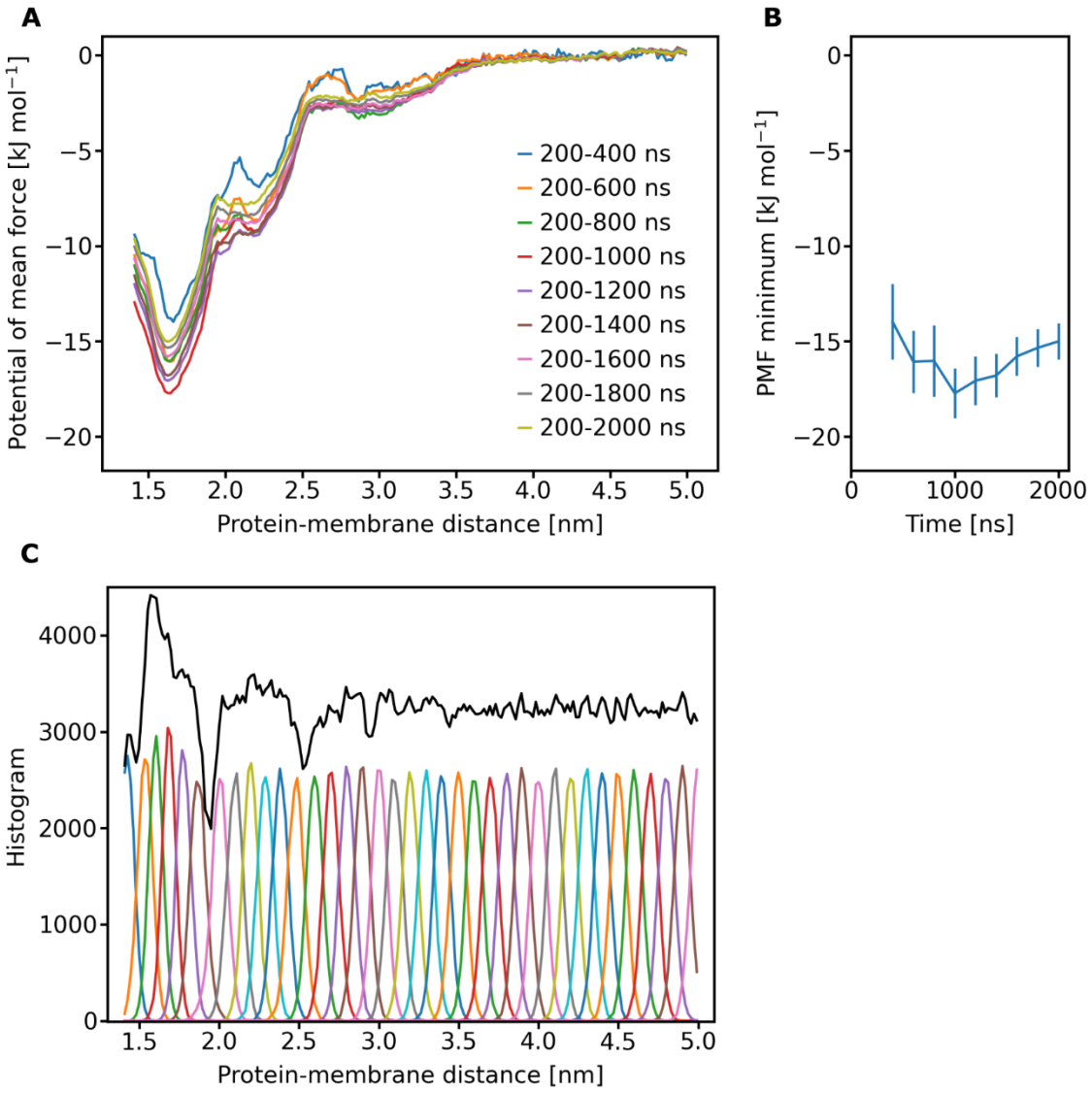

Fig. S11. Convergence analysis of the PMF calculation for R301A tubbyCT binding to two PI(4,5)P_2 lipids. (a) PMFs calculated for different time windows from 200–400 ns to 200–2000 ns in steps of 200 ns. The initial 200 ns of each window were discarded to allow the system to equilibrate. The PMF of the final time interval of 200–2000 ns is used for further analysis. (b) Energy minima from the time windows in (a) including the respective error bars. (c) Histograms of the umbrella windows (colored lines) analyzed by the *gmx wham* tool. The black line depicts the sum of the analyzed histograms.

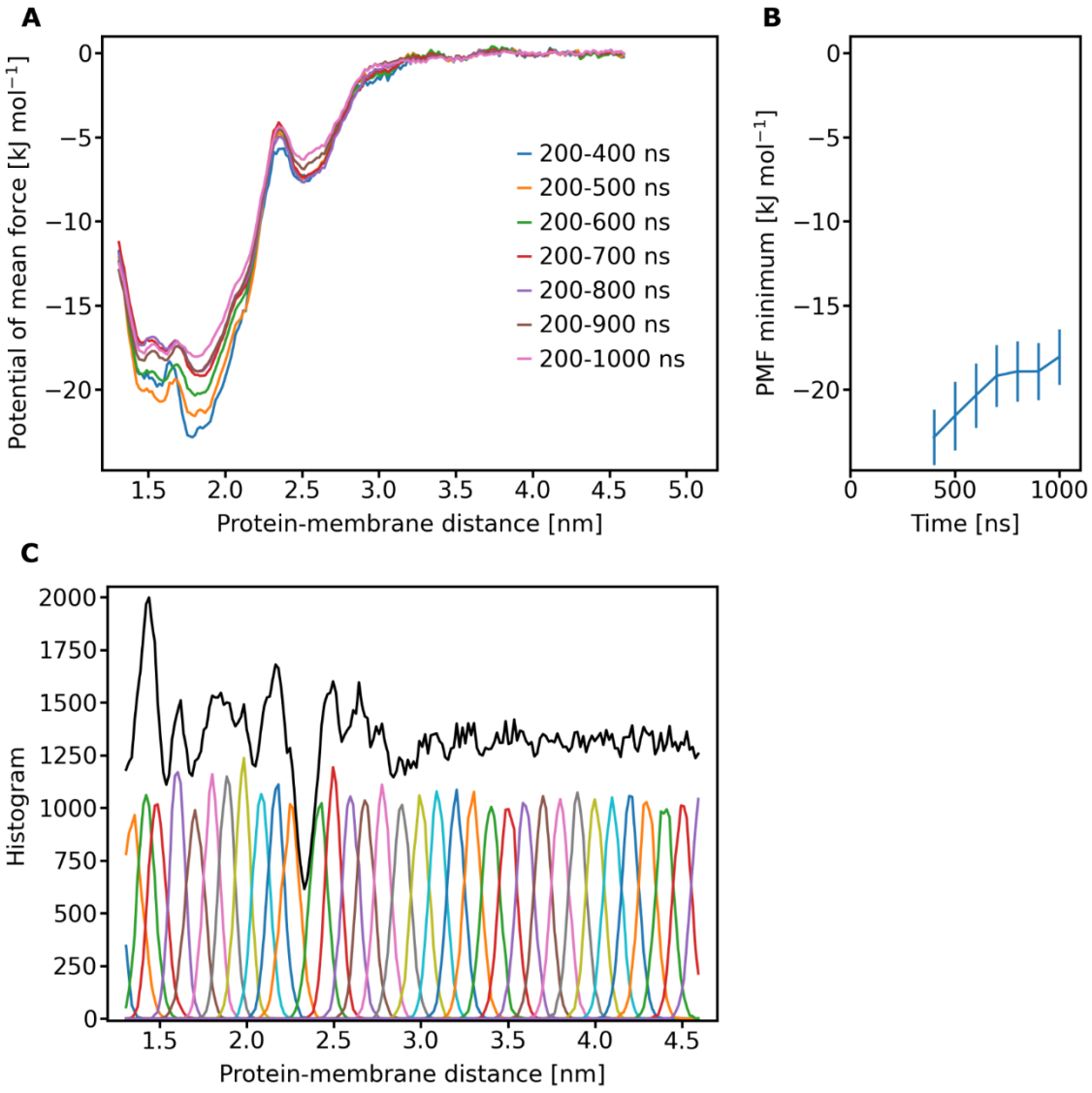

Fig. S12. Convergence analysis of the PMF calculation for PLC-δ1 PH domain to one PI(4,5)P_2 lipid. (a) PMFs calculated for different time windows from 200–400 ns to 200–1000 ns in steps of 100 ns. The initial 200 ns of each window were discarded to allow the system to equilibrate. The PMF of the final time interval of 200–1000 ns is used for further analysis. (b) Energy minima from the time windows in (a) including the respective error bars. (c) Histograms of the umbrella windows (colored lines) analyzed by the *gmx wham* tool. The black line depicts the sum of the analyzed histograms.

Table S1.

Changes of the CG bead types to adapt the CG models of $PI(4,5)P_2$ and PI(4)P from Martini 2 to the open-beta version of Martini 3. Bonded terms were kept unchanged.

$PI(4,5)P_2$				PI(4)P			
id	bead name	bead type Martini 2	bead type open-beta Martini 3	id	bead name	bead type Martini 2	bead type open-beta Martini 3
1	C1	P1	SP1	1	C1	P1	SP1
2	C2	P1	SP1	2	C2	P1	SP1
3	C3	P1	SP1	3	C3	P4	SP3
4	PO4	Qa	Q1	4	PO4	Qa	Q1
5	P4	Qa	Q2	5	P4	Qa	Q2
6	P5	Qa	Q2	6	GL1	Na	N2a
7	GL1	Na	N2a	7	GL2	Na	N2a
8	GL2	Na	N2a	8	C1A	C1	C1
9	C1A	C1	C1	9	D2A	C3	C3
10	D2A	C3	C3	10	C3A	C1	C1
11	C3A	C1	C1	11	C4A	C1	C1
12	C4A	C1	C1	12	C1B	C1	C1
13	C1B	C1	C1	13	C2B	C1	C1
14	C2B	C1	C1	14	C3B	C1	C1
15	C3B	C1	C1	15	C4B	C1	C1
16	C4B	C1	C1				

Table S2.

List of abbreviations used in the manuscript.

Abbreviation	Expression
ARNO	ADP-Ribosylation factor Nucleotide-binding site Opener
ASAP	ASter-Associated Protein
CG	Coarse-Grained
CHO	Chinese Hamster Ovary
DAG	Diacylglycerol
ENTH	Epsin N-Terminal Homology
ER	Endoplasmic Reticulum
E-Syt	Extended Synaptotagmin
FYVE	Fab1, YOTB, Vac1, EEA1
GFP	Green Fluorescent Protein
GPCR	G Protein-Coupled Receptor
GRP	General Receptor for Phosphoinositides
IFT-A	Intraflagellar Transport complex A
IP_3	Inositol-(1,4,5)-trisphosphate
MD	Molecular Dynamics
PG	Phosphatidylglycerol
PH	Pleckstrin Homology
PI	Phosphoinositide
PI(4)P	Phosphatdylinositol-4-phosphate
$PI(4,5)P_2$	Phosphatidylinositol-(4,5)-bisphosphate
PIP_3	Phosphatidylinositol-(3,4,5)-trisphosphate
PLC	Phospholipase C
PM	Plasma Membrane
PMF	Potential of Mean Force
POPC	1-palmitoyl-2-oleoyl-sn-glycero-3-phosphocholine
POPG	1-palmitoyl-2-oleoyl-sn-glycero-3-phosphoglycerol
POPS	1-palmitoyl-2-oleoyl-sn-glycero-3-phosphoserine
PS	Phosphatidylserine
PX	Phox
RFP	Red Fluorescent Protein
RMSF	Root Mean Square Fluctuations
SEM	Standard Error of the Mean
TIRF-M	Total Internal Reflection Fluorescence Microscopy
tubbyCT	C-terminal domain of tubby
TULP	Tubby-Like Protein
VSP	Voltage-Sensitive Phosphatase
WT	Wild Type

Table S3.
Mutagenesis primers for the characterized tubbyCT mutants.

Mutation	Forward primer	Reverse primer
R301A	cctcctggcgggcgcgaagagaaagaagag	ctcttctttctcttcgcgcccgccaggagg
R303A	cctggcgggcaggaaggcaaagaagagtaaaac	gttttactcttctttgccttcctgcccgccagg
K304A	gcgggcaggaagagagcgaagagtaaaacttcc	ggaagttttactcttcgctctcttcctgcccgc
K305A	cgggcaggaagagaaaggcgagtaaaacttcc	ggaagttttactcgcctttctcttcctgcccg
R301A K304A	gcgggcgcgaagagagcgaagagtaaaacttcc	ggaagttttactcttcgctctcttcgcgcccgc
R303A K305A	gcgggcaggaaggcaaaggcgagtaaaacttcc	ggaagttttactcgcctttgccttcctgcccgc
R303A K304A K305A	gcgggcaggaaggcagcggcgagtaaaacttcc	ggaagttttactcgccgctgccttcctgcccgc
R301A R303A K304A K305A	gcgggcgcgaaggcagcggcgagtaaaacttcc	ggaagttttactcgccgctgccttcgcgcccgc